Magneto-optic spectra and the dielectric tensor elements of bismuth-substituted iron garnets at photon energies between 2.2–5.2 eV

S. Wittekoek, T. J. A. Popma, J. M. Robertson, and P. F. Bongers
Philips Research Laboratories, Eindhoven, The Netherlands
(Received 21 October 1974)

Optical and magneto-optical measurements have been performed at room temperature on both polycrystalline samples and thin single-crystal films of bismuth-substituted iron garnets. Kerr rotation, ellipticity, and reflectivity are given for polycrystalline samples of composition $Y_{3-x}Bi_xFe_5O_{12}$ ($0 < x \leq 1$) between 2.0 and 5.2 eV (wavelengths between 0.6 and 0.24 μm). The absorption and the Faraday rotation and ellipticity of epitaxial films with $0 < x < 0.5$ were measured up to 3.5 eV. The experimental results have been used to calculate the diagonal and off-diagonal elements of the dielectric tensor at optical frequencies. Strong magneto-optic active transitions have been found at 2.8, 3.3, 4.1, and 4.9 eV, apart from the weaker crystal-field transitions. The bands at 2.8 and 3.3 have been studied in more detail: The oscillator strengths and splittings due to spin-orbit coupling were calculated, both increase with bismuth substitution. The large splitting of the band at 3.3 eV for the bismuth-substituted compounds is concluded to be the origin of the anomalous Faraday rotation of these compounds. The assignment of these bands in terms of an energy level scheme is discussed.

I. INTRODUCTION

Substitution of bismuth ions in yttrium and rare-earth iron garnets ($R_3Fe_5O_{12}$) enhances strongly the Faraday and Kerr rotation in the visible[1,2] and near infrared.[3] This seemed at variance with the idea that these magneto-optic effects could be explained by optical transitions involving only the iron and oxygen ions[4–6] and lead therefore to new investigations of the optical transitions above 3 eV in these materials.[7]

A first step in such investigations should be the calculation of the elements of the dielectric tensor $\hat{\epsilon}$ at optical frequencies[5,8] from optical observables such as reflection, Kerr rotation, etc. These tensor elements are functions of the matrix elements of optical transitions and the spin-orbit splitting of excited states. Therefore, the main purpose of this work is to establish the elements of $\hat{\epsilon}$ for bismuth-substituted iron garnets at photon energies up to 5 eV. Most previous work consisted of absorption and Faraday-rotation measurements on iron garnets without bismuth in the region below 2.5 eV and the elements of $\hat{\epsilon}$ for unsubstituted $Y_3Fe_5O_{12}$ (YIG).[5,9] No determination of the dielectric tensor elements of the bismuth-substituted iron garnets has been reported so far.

In the present work magneto-optical data are derived from two sets of experiments. In the first, Kerr-rotation, -ellipticity, and -reflection measurements are performed on a series of polycrystalline samples of $Y_{3-x}Bi_xFe_5O_{12}$ ($0 \leq x \leq 1$). From these data the tensor elements ϵ_0 and ϵ_1 are determined between 2.5 and 5 eV. Secondly, the Faraday rotation and ellipticity and absorption of thin single-crystal films of $Y_{3-x}Bi_xFe_5O_{12}$ ($x < 0.5$) grown on $Gd_3Ga_5O_{12}$ substrates are determined. By combining the results of the two types of experiments it is possible to determine with high accuracy the optical and magneto-optical constants from 1.8–5 eV.

The results should be interpreted in terms of an energy-level scheme of the iron garnets, which is done in Sec. VI D, where special attention is given to intervalence transitions.

II. MAGNETO-OPTIC EFFECTS AND THE DIELECTRIC TENSOR

We will discuss briefly the relations between the observed magneto-optic quantities and the dielectric tensor elements, which are used in the analysis of the experimental data. More extended treatments can be found in Ref. 8.

The propagation of electromagnetic waves in a material can be described by the electric and magnetic permeability tensors $\hat{\epsilon}$ and $\hat{\mu}$. At optical frequencies $\hat{\mu}$ may be taken equal to unity. For a geometry with a cubic material and a magnetization parallel to the z axis, the dielectric tensor has the form

$$\hat{\epsilon} = \begin{pmatrix} \epsilon_0 & +i\epsilon_1 & 0 \\ -i\epsilon_1 & \epsilon_0 & 0 \\ 0 & 0 & \epsilon_z \end{pmatrix}. \tag{1}$$

All elements have a real and imaginary part:

$$\epsilon_j = \epsilon_j' + i\epsilon_j'' .$$

The diagonal element ϵ_0 is related to the normal refractive index n and the normal extinction coefficient k by

$$n^2 - k^2 = \epsilon_0' \quad \text{and} \quad 2nk = \epsilon_0'' . \tag{2}$$

The off-diagonal element is related to the refractive indices $n_\pm$ and the extinction coefficients $k_\pm$ of right

(+) and left (−) circularly polarized radiation (RCP and LCP) by

$$(n_+ - n_-) + i(k_+ - k_-) = \epsilon_1/\epsilon_0^{1/2} . \quad (3)$$

The Faraday rotation Θ_F which is half the phase difference between the RCP and LCP waves equals

$$\Theta_F = \frac{\pi(n_+ - n_-)}{\lambda} = \mathrm{Re}\left(\frac{\pi\epsilon_1}{\lambda\epsilon_0^{1/2}}\right) . \quad (4)$$

The Faraday ellipticity η_F is proportional to the difference in absorption of the RCP and LCP waves:

$$\eta_F = \frac{\pi}{\lambda}(k_+ - k_-) = \mathrm{Im}\left(\frac{\pi\epsilon_1}{\lambda\epsilon_0^{1/2}}\right) . \quad (5)$$

Reversely, ϵ_1' and ϵ_1'' can be expressed in terms of the observable quantities

$$\epsilon_1' = (\lambda/\pi)(n\Theta_F - k\eta_F) , \quad (6)$$

$$\epsilon_1'' = (\lambda/\pi)(k\Theta_F + n\eta_F) . \quad (7)$$

The Kerr rotation φ_K equals half the difference between the phase shifts of RCP and LCP light after reflection and can be shown to be

$$\varphi_K = \tfrac{1}{2}(\varphi_+ - \varphi_-) = \mathrm{Im}\left(\frac{\hat{r}_+ - \hat{r}_-}{\hat{r}_+ + \hat{r}_-}\right) , \quad (8)$$

where $\hat{r}_\pm = r_\pm e^{i\varphi_\pm}$ are the complex reflection coefficients. We have assumed that

$$(r_+ - r_-)/(r_+ + r_-) \ll 1 .$$

The Kerr ellipticity equals the ratio of minimum and maximum amplitude of the reflected light:

$$\eta_K = -\frac{r_+ - r_-}{r_+ + r_-} = \mathrm{Re}\left[-\left(\frac{\hat{r}_+ - \hat{r}_-}{\hat{r}_+ + \hat{r}_-}\right)\right] . \quad (9)$$

ϵ_1' and ϵ_1'' can be expressed in φ_K and η_K:

$$\epsilon_1' = -\varphi_K(3n^2k - k^3 - k) - \eta_K(n^3 - 3n^2k - n) , \quad (10)$$

$$\epsilon_1'' = \varphi_K(n^3 - 3nk^2 - n) - \eta_K(3n^2k - k^3 - k) . \quad (11)$$

III. EXPERIMENTAL DETAILS

A. Samples

As mentioned in the Introduction both polycrystalline samples and epitaxially grown single-crystal films were used in the experiments.

The preparation of the polycrystalline materials of $Y_{3-x}Bi_xFe_5O_{12}$ is described extensively in Ref. 10. Briefly, cylindrical disks of ~2 cm diameter and a few mm thick were prepared by the standard ceramic techniques of milling and sintering. Since the samples were used for reflection experiments, special care was taken to obtain undamaged surfaces. Therefore, the materials were Syton polished and annealed afterwards.

The preparation of the bismuth-containing-iron-garnet films by liquid-phase epitaxy (LPE) is described in Ref. 11. Most measurements were performed on films of $Y_{3-x}Bi_xFe_5O_{12}$ on $Gd_3Ga_5O_{12}$ substrates with $x \leq 0.3$. Higher bismuth concentrations could be realized in rare-earth iron garnets with small rare-earth ions.[12] Therefore, measurements were also done on a film of $Y_{1.0}Lu_{1.4}Bi_{0.6}Fe_5O_{12}$. For the present experiments films were chosen for which the incorporation of Pb from the flux was kept as low as possible by choosing proper growth rates. Since the transmission and Faraday-rotation measurements were performed at short wavelengths (down to 330 nm) films of about 0.1 μm thickness were necessary. Some films were thinned down to the desired thickness by argon-ion sputtering.

B. Optical measurements

Both Faraday- and Kerr-effect measurements were performed with polarization modulation techniques allowing a determination of the rotation angles with an accuracy of better than 0.001°. The apparatus for the Kerr-effect measurements was similar to that described earlier,[13] but modified to extend the spectral range into the uv. A 450-W xenon arc lamp was used as light source and Glan Thompson prisms with air gaps as polarizers. Below 300 nm a Philips Solar Blind photomultiplier was employed as detector to eliminate stray light from the visible region. This allowed accurate measurements down to 240 nm to be performed.

The ellipticity measurements (both Faraday and Kerr) as a function of wavelength were done using a Soleil-Babinet compensator.

Since the surfaces of all samples were rather large (>1 cm^2) the reflection measurements could be performed on a Beckman DK 2A spectrophotometer with a reflectance accessory. It was anticipated that at very short wavelengths (240 nm) the measured reflection coefficients could be too low due to surface irregularities. To correct for this effect the samples were covered after the measurements with an evaporated layer of aluminum. The reflection of this Al layer was then compared with that of a specular mirror of evaporated Al on glass. The necessary corrections however, were never larger than 10%.

IV. EXPERIMENTAL RESULTS

A. Kerr effect

Figures 1 and 2 show the results of Kerr-rotation and -ellipticity measurements on the polycrystalline samples of $Y_{3-x}Bi_xFe_5O_{12}$ ($0 \leq x \leq 1$). The data were taken between 1.8 and 5.2 eV in a saturating magnetic field of 2 kOe and are displayed as double rotations and ellipticities, i.e., $\varphi = \varphi_K(\vec{M}) - \varphi_K(-\vec{M}) = 2\varphi_K$, where $\vec{M}$ is the magnetization. The rotation shows positive or negative peaks when the ellipticity passes through zero and vice versa in accordance with the Kramers-Kronig relations.

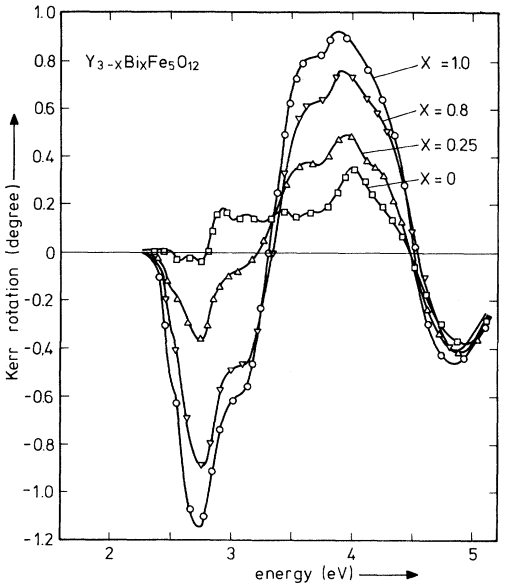

FIG. 1. Kerr-rotation spectra of polycrystalline $Y_{3-x}Bi_xFe_5O_{12}$.

The results for YIG ($x=0$) are similar to those obtained by Kahn *et al.*,[5] but some structure at photon energies below 3 eV is resolved better in the present curves. Some of the sharp peaks in YIG disappear gradually when the bismuth substitution is increased. The most remarkable effect, however, is the strong increase of the Kerr rotation near 2.7 and 3.7 eV and the Kerr ellipticity near 2.4 and 3.4 eV.

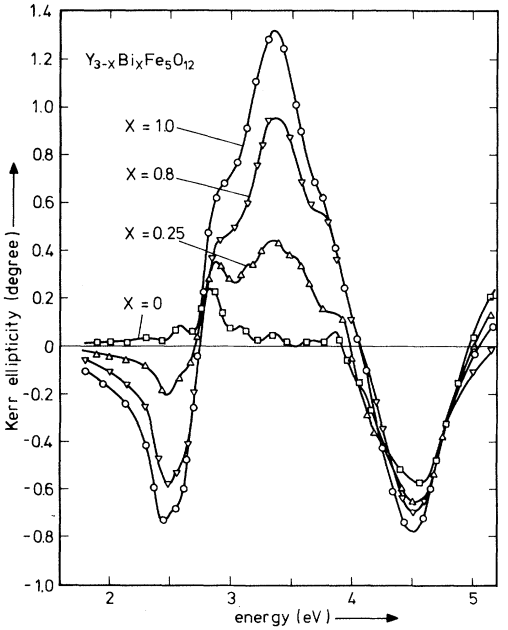

FIG. 2. Kerr-ellipticity spectra of polycrystalline $Y_{3-x}Bi_xFe_5O_{12}$.

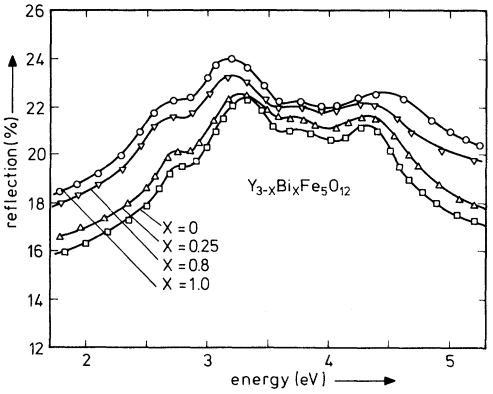

FIG. 3. Reflectivity spectra of $Y_{3-x}Bi_xFe_5O_{12}$.

B. Reflectivity data

The results for the straight reflectivity measurements between 1.8 and 5.5 eV on these polycrystalline samples are shown in Fig. 3. These data were used to calculate the optical constants n and k and the diagonal elements of the dielectric tensor $\epsilon_0' + i\epsilon_0''$ [cf. Eqs. (2) and (3)] with the aid of a Kramers-Kronig analysis related to that suggested first by Roessler.[14] For this method one needs as input data (i) the reflectivity data over a wide photon energy range and (ii) at two wavelengths in this interval the value of the phase angle θ of the complex (amplitude) reflection coefficient

$$\sqrt{R}\, e^{i\theta},$$

which is related to the optical constants n, k, and R by

$$\theta = \arcsin \frac{1-R}{2\sqrt{R}} \frac{k}{n}. \tag{12}$$

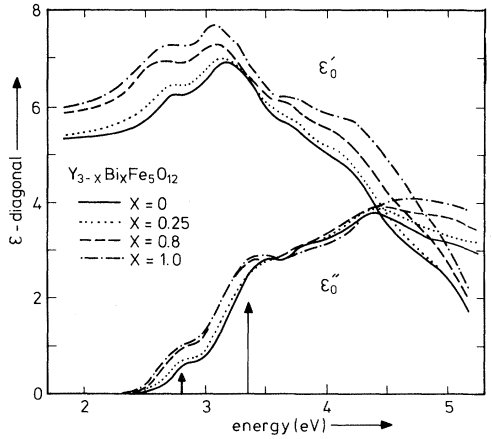

FIG. 4. Diagonal elements ϵ_0' and ϵ_0'' of the dielectric tensor of $Y_{3-x}Bi_xFe_5O_{12}$.

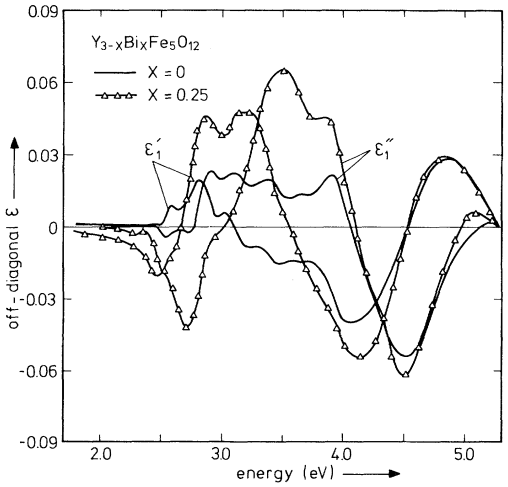

FIG. 5. Off-diagonal tensor elements ϵ_1' and ϵ_1'' for $Y_{3-x}Bi_xFe_5O_{12}$, for $x=0$ and $x=0.25$.

In a first approximation fairly accurate values of ϵ_0' and ϵ_0'' (or, equivalently n and k) can be obtained by taking $k=0$ and thus $\theta=0$ at two photon energies below the absorption edge, at 1.9 and 2.3 eV. We could improve on this first approximation by using for k at 1.9 and 2.3 eV values estimated from our transmission data on thin films. The spectra of ϵ_0' and ϵ_0'' resulting from the Kramers-Kronig analysis are shown in Fig. 4.

C. Off-diagonal elements

From the values of ϵ_0' and ϵ_0'' and the measured Kerr effects the off-diagonal elements ϵ_1' and ϵ_1'' were calculated using Eqs. (2), (3), (10), and (11). The results are shown in Fig. 5 for $x=0$ and $x=0.25$ and in Fig. 6 for $x=0.8$ and $x=1.0$. In YIG we note clear extrema of ϵ_1' at 2.8, 4.1, and 4.9 eV, and a number of weaker structures. When bismuth is added ϵ_1' increases, especially near 2.4 and 3.3 eV where new peaks develop. For $x=1.0$, ϵ_1' reaches a peak value of 0.18 at about 3.3 eV compared with $\epsilon_1'=0.02$ for $x=0$. Near 2.4 eV, ϵ_1' changes from 0 to -0.10 and near 4 eV from -0.05 to 0.08 when x goes from 0 to 1.0. It may be noted that for YIG the results agree well with those of Kahn *et al.*[5] The small discrepancy can be attrib-

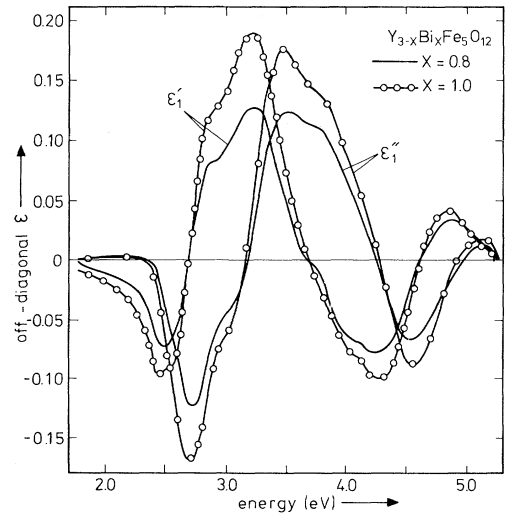

FIG. 6. Off-diagonal tensor elements ϵ_1' and ϵ_1'' for $Y_{3-x}Bi_xFe_5O_{12}$, for $x=0.8$ and $x=1.0$.

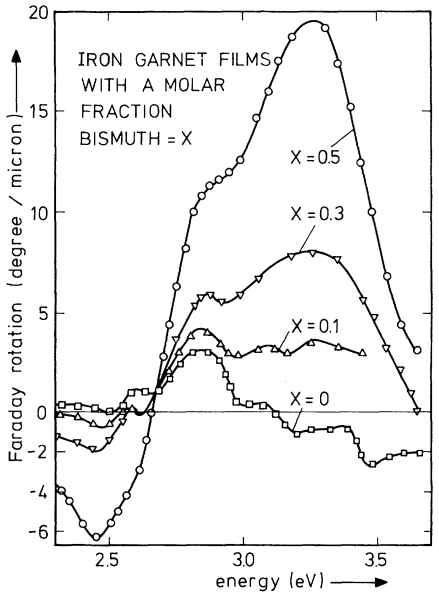

FIG. 7. Faraday-rotation spectra of LPE films of bismuth-substituted YIG, x = molar fraction bismuth.

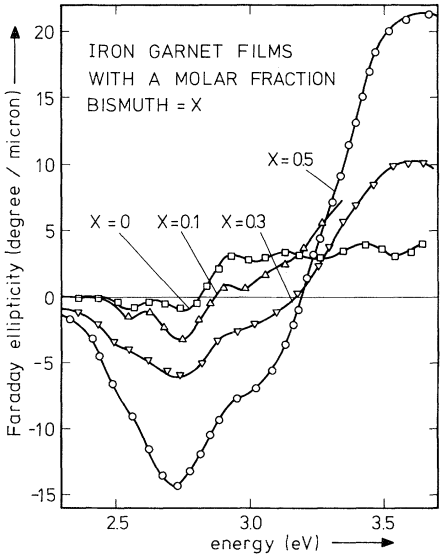

FIG. 8. Faraday-ellipticity spectra of LPE films of bismuth-substituted YIG, x = molar fraction bismuth.

TABLE I. Composition of garnet films grown by liquid-phase epitaxy and used in the experiments.

Film composition	Indication in figures and text
$Y_3Fe_5O_{12}$	$x=0$
$Y_{2.9}Bi_{0.1}Fe_5O_{12}$	$x=0.1$[a]
$Y_{2.6}Bi_{0.3}Pu_{0.1}Fe_5O_{12}$	$x=0.3$
$Y_{1.0}Lu_{1.4}Bi_{0.5}Pb_{0.1}Fe_5O_{12}$	$x=0.5$

[a]Made from a lead-free flux, see Ref. 5.

uted to the more accurate values of the present reflection data.

D. Thin-film measurements

The Faraday rotation and ellipticity of four thin iron-garnet films are shown in Figs. 7 and 8. The composition of these LPE films are given in Table I. The data have been corrected for the rotation from the substrate and for the influence of the reflections at the film-air and film-substrate interfaces. The Faraday-rotation data for YIG up to 2 eV are in good agreement with those reported earlier by Wettling *et al.*[15] The bismuth substitution leads in the Faraday-rotation spectra to the development of two new peaks at, respectively, 2.4 and 3.3 eV. At the latter photon energy a maximum rotation of about $20°/\mu m$ was observed for $x=0.5$, which is the highest value reported so far for ferric oxides. The absorption spectra of the films are shown in Fig. 9. Two effects are observed in these spectra: (i) two absorption maxima exist near 2.8 and 3.4 eV for all films and (ii) the absorption increases noticeably with increasing bismuth substitution. In Fig. 10 the k values of the pure YIG film are compared with those resulting from the Kramers-Kronig analysis of the polycrystalline YIG sample. Sharp crystal-field absorp-

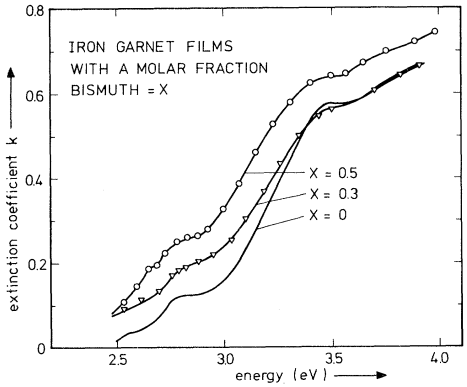

FIG. 9. Extinction coefficient k versus photon energy for LPE films of bismuth-substituted YIG.

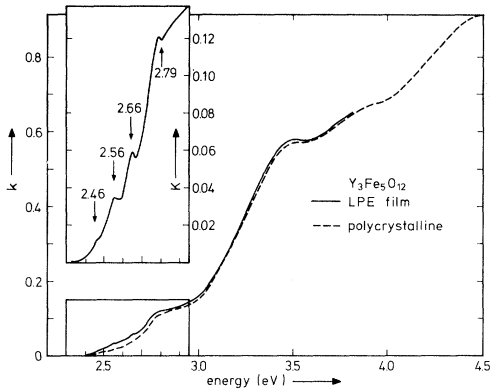

FIG. 10. Comparison of the extinction coefficients of polycrystalline (----) and expitaxially grown $Y_3Fe_5O_{12}$. The data for the polycrystalline sample were obtained from a Kramers-Kronig analysis of reflectivity data.

tions are observed in the transmission experiments on the thin film at 2.46, 2.56, 2.66, and 2.79 eV (see inset of Fig. 10) which are not found by the Kramers-Kronig analysis, but for the broad and intensive maxima the agreement is very good.

With the aid of the Faraday-rotation and -ellipticity measurements of Figs. 7 and 8 and the results of absorption and reflection measurements, the off-diagonal elements ϵ_1' and ϵ_1'' of the garnet films were calculated using Eqs. (6) and (7). The results are shown in Figs. 11 and 12. In Fig. 13 we compare again the ϵ_1 spectra for the pure YIG film with the ϵ_1 spectra resulting from Kerr-effect measurements on polycrystalline YIG. It is satisfying that the results obtained by different experimental techniques and on polycrystalline materials and LPE films show such good agreement. This indicates that data such as given in Fig. 13 form a reliable experimental basis for an analysis of the energy-level spectrum of YIG.

In Fig. 13 we have also indicated the centers of optical transitions as they follow from the magneto-optical measurements; these will be discussed further in Sec. V.

For the bismuth-substituted films the same trend is observed as for the polycrystalline samples viz. the development of a strong positive peak at 3.3 eV and a weaker at 2.4 eV. No detailed quantitative comparison between bismuth-containing films and polycrystalline materials is possible since they do not have exactly the same compositions.

V. MICROSCOPIC THEORY OF THE DIELECTRIC TENSOR

The spectra of the diagonal (ϵ_0) and off-diagonal (ϵ_1) terms of the dielectric tensor as presented in Sec. IV allow an interpretation of the experimental results in terms of a microscopic theory which relates ϵ_0 and ϵ_1 to energy-level splittings and

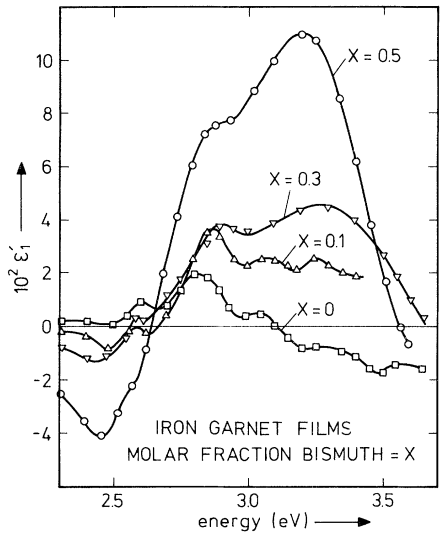

FIG. 11. The off-diagonal tensor element ϵ_1' for thin films of bismuth-substituted YIG, calculated with the data from Figs. 7–11.

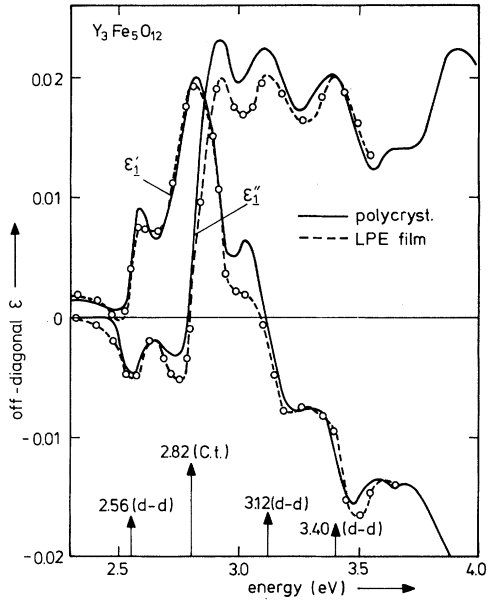

FIG. 13. Comparison of the off-diagonal dielectric tensor elements ϵ_1' and ϵ_1'' calculated from transmission measurements on a thin film (Figs. 7–11) and from reflection measurements on a polycrystalline sample of $Y_3Fe_5O_{12}$ (Fig. 3). The energies where charge transfer (CT) or crystal field (d-d) transitions occur are indicated by arrows.

transition probabilities. We will consider two types of optical transitions.

A. Type I: double transitions

Consider first a spin- and electric-dipole-allowed transition between an orbital singlet ground state and an excited state which is split by the combined effect of exchange field and spin-orbit coupling. To these transitions, often referred to as "double transitions," belong spin-allowed charge transfer bands. It can be shown[16] that for these transitions ϵ_1 behaves as

$$\epsilon_1 = \frac{\omega_p^2 f \Delta L}{2\omega_0} \frac{(\omega_0-\omega)^2 - \Gamma_0^2 + 2i\Gamma_0(\omega_0-\omega)}{[(\omega_0-\omega)^2+\Gamma_0^2]^2} . \qquad (13)$$

Δ is the separation between the levels because of spin-orbit coupling, ω_0 and Γ_0 are the center frequency and halfwidth at half-height of the transition, and it is assumed that $\Delta \ll \Gamma_0$. $\omega_p^2 = 4\pi Ne^2/m$, where e and m are the electronic charge and mass and N is the number of octahedral Fe^{3+} ions per cm^3. f is the oscillator strength defined as $f = (2m\omega_0/Le^2)|p_e^x|^2$, where p_e^x is the electric dipole matrix element, between ground and excited state. L is the Lorentz-Lorenz local field correction which equals $[(n^2+2)/3]^2$.

The real part of ϵ_1 shows a bell-shaped behavior passing through zero at $\omega = \omega_0 \pm \Gamma$. The imaginary part ϵ_1'' shows a dispersive behavior around ω_0. These shapes, illustrated in Fig. 14, are often referred to as "diamagnetic behavior" for historical reasons.[17] At $\omega = \omega_0$, $\epsilon_1'' = 0$ and ϵ_1' has a maximum value

$$(\epsilon_1')_{max} = -(\omega_p^2 \Delta f L/2\omega_0\Gamma_0^2) . \qquad (14)$$

The diagonal elements ϵ_0 show also a resonant behavior around ω_0. The imaginary part ϵ_0'' shows a maximum at $\omega = \omega_0$ given by

$$(\epsilon_0'')_{max} = \omega_p^2 f L/2\omega_0\Gamma_0 . \qquad (15)$$

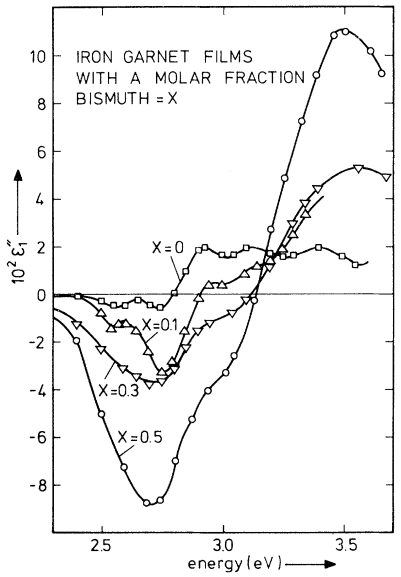

FIG. 12. The off-diagonal tensor element ϵ_1'' for thin films of bismuth-substituted YIG.

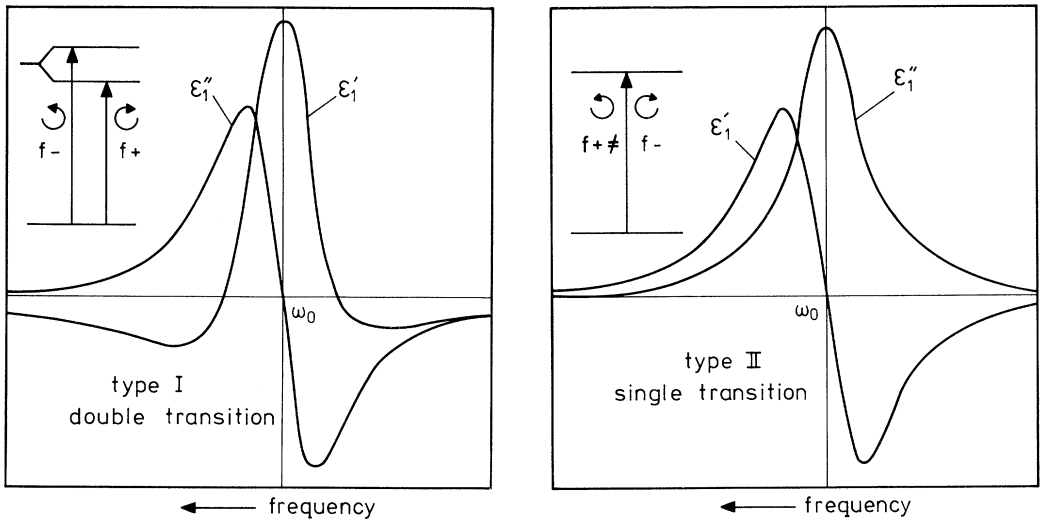

FIG. 14. The calculated spectra of ϵ_1' and ϵ_1'' for a so-called double transition with a "diamagnetic" line shape (type I) and for a so-called single transition with a "paramagnetic" line shape (type II).

B. Type II: single transitions

The second type of transitions are the so-called "single transitions." In this case neither the ground state nor the final state are split but the oscillator strengths f^+ and f^- for, respectively, RCP and LCP light are different. Examples of type-II transitions are the spin- and electric-dipole-forbidden crystal-field transitions of Fe^{3+} ions.

A specific example of this effect has been treated by Clogston.[18] The contribution to ϵ_1 for such a band can be shown to be

$$\epsilon_1 = \frac{\omega_p^2 f df L}{2} \frac{\omega(\omega_0^2 - \omega^2 - \Gamma_0^2) + i\Gamma_0(\omega_0^2 + \omega^2 + \Gamma_0^2)}{\omega_0[(\omega_0^2 + \omega^2 + \Gamma_0^2)^2 + 4\omega^2\Gamma_0^2]}, \tag{16}$$

where the fractional dichroism df is defined as

$$df = \frac{f_- - f_+}{f_- + f_+} = \frac{f_- - f_+}{2f}. \tag{17}$$

For these type-II transitions the real part ϵ_1' has a dispersive shape around $\omega \approx \omega_0$ and ϵ_1'' a dissipative behavior. Both are illustrated in Fig. 14. The ϵ_1' curve is often referred to as the "paramagnetic" shape. The marked difference in the shape between type-I and type-II transitions is useful for interpretation of experimental spectra. At $\omega = \omega_0$, $\epsilon_1' = 0$ and ϵ_1'' has a maximum value

$$(\epsilon_1'')_{\max} = \frac{\omega_p^2 f df L}{\omega_0} = df(\epsilon_0'')_{\max}. \tag{18}$$

VI. DISCUSSION

A. Single transitions below 3.5 eV

With the aid of the previous summary we investigate the spectra of ϵ_1' and ϵ_1'', starting with those of unsubstituted YIG below 3.5 eV as shown in Fig. 13. We observe three type-II (single) transitions at 2.56, 3.12, and 3.40 eV. In Table II the essential data of all crystal-field transitions are summarized, as derived from the formulas given above.

TABLE II. Measured and calculated properties of single transitions below 3.5 eV.

Transition energy $\hbar\omega$ (eV)	Type of transition	Rotation $(\epsilon_1'')_{\max}$	Width Γ (eV)	Absorption $(\epsilon_0'')_{\max}$	Fractional dichroism df
2.46	$^6A_1 \rightarrow {}^4T_2$				0.0
2.56	$^6A_1 \rightarrow {}^4E, {}^4A_1$	−0.004	0.04	0.04	0.1
2.66	$^6A_{1g} \rightarrow {}^4E_g, {}^4A_{1g}$				0.0
2.79	$^6A_{1g} \rightarrow {}^4T_{2g}$				0.0
3.12		+0.008	0.09		
3.40		+0.009	0.09		

TABLE III. Measured and calculated properties of the absorption band I at 2.8 eV in iron garnets for various bismuth contents.

						Normalized increases	
Bismuth content	Absorption $(\epsilon_0'')_{max}$	Width Γ (eV)	Oscillator strength f	Rotation $(\epsilon_1')_{max}$	Splitting Δ (eV)	f_{Bi} [c]	Δ_{Bi} [c] (eV)
$x=0$ LPE[a]	0.26	0.08	1.2×10^{-3}	0.014	0.0043		
$x=0$ pol[b]	0.25	0.09	1.4×10^{-3}	0.014	0.0049		
$x=0.25$ pol	0.34	0.11	2.0×10^{-3}	0.026	0.0084	0.0040	(0.009)
$x=0.5$ LPE	0.38	0.12	2.5×10^{-3}	0.030	0.0095	0.0036	(0.008)
$x=0.8$ pol	0.45	0.15	3.7×10^{-3}	0.045	0.015	0.0040	0.012
$x=1.0$ pol	0.46	0.17	4.1×10^{-3}	0.050	0.019	0.0042	0.016

[a]LPE film.

[b]Polycrystalline.

[c]f_{Bi} and Δ_{Bi} give the increases of f and Δ, respectively, due to bismuth normalized for one Bi ion per unit cell (see text).

Evidently only the transition ${}^6A_1 \rightarrow {}^4E, {}^4A_1$ at 2.56 eV is observed both in the rotation and absorption spectrum. This allows a calculation of the fractional dichroism of this peak using formulas of Sec. V B. We estimate from the absorption that $(\epsilon_0'')_{max}=0.04$, which results in $df=0.1$ after applying Eq. (18). The transitions at 2.46, 2.66, and 2.79 have such small fractional dichroism df that they are not observed as peaks in the magneto-optic spectrum.

On the other hand, the peaks at 3.12 and 3.40 eV have no clear analog in the absorption spectrum. Wemple *et al.*[9] and Scott *et al.*[19] argue that in this spectral region absorption bands are present which cannot be observed as separate peaks, but which result from a computer analysis of the spectrum. These bands however have widths of about 0.15 eV which is too high to be identified with the rotational peaks at 2.56 and 3.12 eV. We conclude that these rotational peaks are from crystal-field transitions which are not observed in absorption spectra because they are situated on the steep wings of other stronger transitions such as charge transfer bands. The crystal-field transitions become less distinguishable in both ϵ_0 and ϵ_1 spectra with increasing Bi content (Figs. 4–6).

B. Double transitions

In the photon energy region below about 3.4 eV some strong transitions can be distinguished in both the ϵ_0 and ϵ_1 spectra (Figs. 4, 5, 9, and 13).

In the ϵ_1 spectrum of YIG (Fig. 13) we distinguish clearly a type-I transition at about 2.8 eV. In the spectrum of ϵ_0'' we distinguish two broad maxima corresponding to bands at 2.8 and 3.4 eV which we define as bands I and II, respectively. By analyzing the ϵ_0'' curve we estimate for band I $(\epsilon_0'')_{max}=0.25$ and the linewidth $\Gamma=0.09$ eV and for band II $(\epsilon_0'')_{max}=1.1$ and $\Gamma=0.22$ eV.

We associate the maximum of ϵ_1' near 2.8 eV (Fig. 13) with the band I found in absorption (Figs. 4 and 9). From the observed value of $(\epsilon_1')_{max}=0.014$ we derive with Eqs. (14) and (15) a splitting of the excited state of band I, $\Delta=0.008$ eV. For band II, although intenser than band I, no corresponding maximum of ϵ_1' is observed. We conclude, therefore, that in unsubstituted YIG the splitting of the excited state is essentially zero for band II at 3.4 eV. The essential data of bands I and II are given in Tables III and IV. The results are accurate within about 20% due to overlap effects.

The spectra of ϵ_0'' and k for the bismuth-substituted samples (Figs. 4 and 9) shows a broadening and slight increase of oscillator strength for bands I and II with increasing bismuth substitution. No indication is found for the occurrence of a new transition due to bismuth.

A drastic change occurs in the spectra of ϵ_1 (Figs. 5 and 6), the most striking effect being the development of a strong peak in ϵ_1' at about 3.3 eV. This peak reaches a value of $\epsilon_1'=0.18$ for $x=1.0$ compared with $\epsilon_1'=0.02$ for $x=0$. The maximum near 2.8 eV, associated with band I, is still present, but is observed only as a shoulder on the strong peak near 3.3 eV for the higher Bi concentrations.

We associate the ϵ_1' peak at 3.3 eV with absorption band II found in both YIG and Bi-substituted YIG (Fig. 9). The differences in central frequency between the ϵ_0'' peak (~3.4 eV) and the ϵ_1' peak (~3.3 eV) can be attributed to the influences of the wings of other transitions.

In Tables III and IV we have summarized the data calculated for all available samples at various bismuth concentrations. The bismuth substitution increases the oscillator strengths and the splittings of both bands, but the strongest effect is the increase of the splitting of band II, which was negligibly small for YIG.

TABLE IV. Measured and calculated properties of absorption band II at 3.3 eV in iron garnets with various bismuth contents.

						Normalized increases	
Bismuth content	Absorption $(\epsilon_0'')_{max}$	Width Γ (eV)	Oscillator strength f	Rotation $(\epsilon_1')_{max}$	Splitting Δ (eV)	f_{Bi} [c]	Δ_{Bi} [c] (eV)
$x=0$ LPE[a]	1.02	0.20	0.013	0	0		
$x=0$ pol[b]	1.1	0.24	0.016	0	0		
$x=0.25$ pol	1.1	0.29	0.020	0.05	0.013	0.010	0.032
$x=0.5$ LPE	1.02	0.30	0.017	0.09	0.029	0.012	0.062
$x=0.8$ pol	1.0	0.31	0.019	0.12	0.037	0.011	0.059
$x=1.0$ pol	1.2	0.32	0.023	0.18	0.048	0.010	0.057

[a]LPE film.

[b]Polycrystalline.

[c]f_{Bi} and Δ_{Bi} give the increases of f and Δ, respectively, due to bismuth normalized for one bismuth ion (see text).

We have attempted to establish the bismuth effect somewhat more quantitatively. From the foregoing we derive that there are transitions (I and II) in YIG which involve Fe^{3+} ions for which the parameters f and Δ are changed when a bismuth ion is present in the neighborhood of these Fe^{3+} ions, due to some unknown interaction, e.g., via the oxygen ions.

The influence of Bi^{3+} upon the oscillator strength and splitting of such transitions can be expressed as

$$f=(1-p)f_0+p(f_0+f_{Bi}) , \tag{19}$$

$$f\Delta=p\,(f_0+f_{Bi})(\Delta_0+\Delta_{Bi})+(1-p)f_0\Delta_0 , \tag{20}$$

where f_0 and Δ_0 are the oscillator strength and splitting without the influence of Bi^{3+}, and f_{Bi} and Δ_{Bi} are the increase of oscillator strength and splitting due to the presence of Bi^{3+}. p is the fraction of ions involved in the transition which is influenced by Bi^{3+}, and is in a first approximation proportional to the molar fraction x of Bi.

The values of f_{Bi} and Δ_{Bi} are given in Tables III and IV for bands I and II, respectively, assuming $p=\frac{2}{3}x$, which is the case for O^{2-} ions or Fe_{oct}-Fe_{tetr} pairs. The results are not meaningful for the low bismuth concentrations (values between brackets in Tables III and IV). For the higher bismuth concentrations the values of f_{Bi} and Δ_{Bi} are constant for the various samples. We can conclude from Table II that the incorporation of a bismuth ion close to the Fe^{3+} ions involved in transition I leads to an increase of oscillator strength of $f_{Bi}\approx 0.01$ eV.

For band II these values are $f_{Bi}\approx 0.03$ and $\Delta_{Bi}\approx 0.06$ eV.

In the high-energy region of the ϵ_1 spectrum of YIG (Fig. 5) we note two broad peaks of ϵ_1' of opposite sign at, respectively, 4.1 and 4.9 eV, which have the characteristics of "double" transitions (type I). In the ϵ_0 spectrum (Fig. 4) in the same energy region we observe only weak local maxima of ϵ_0'' as a result of strongly overlapping transitions which lead to an absorption spectrum with a continuous character. The ϵ_1' maxima will be the best indications of the center of bands as far as a discussion in terms of separate bands is possible. The halfwidth of both bands is between 0.2 and 0.3 eV.

The ϵ_1' peak at 4.1 eV increases strongly when bismuth is substituted, from $(\epsilon_1')_{max}=0.04$ for $x=0$ to $(\epsilon_1')_{max}=0.10$ for $x=1.0$. The band at 4.9 increases only weakly.

C. Behavior of ϵ_1' at low photon energies

For photon energies below the absorption edge ($\hbar\omega<2.5$ eV) the Faraday rotation Θ_F is proportional to the dielectric tensor element ϵ_1'. With the aid of the spectra of ϵ_1' given in Figs. 5 and 6 we can now draw some conclusions about the transitions which give the dominant contributions to these "wings" of ϵ_1' and thus, to the Faraday rotation.

For the bismuth substituted garnets, ϵ_1' below 2.5 eV will have the dominant contribution from the wing of band II at 3.3 eV and a smaller contribution from band I (2.8 eV). According to the theoretical line shapes of double transitions as shown in Fig. 14, the curve of ϵ_1' for a positive peak at ω_0 will show a secondary negative peak at about $\omega=\omega_0-\Gamma$. These negative peaks for bands I and II overlap and form the observed negative peak in ϵ_1' near 2.5 eV (Fig. 6). However, the observed magnitude of this minimum at 2.5 eV is larger than expected from the theoretical line shape. This may be explained by the following effect:

The behavior of ϵ_1' of a double transition depends on splitting Δ and the line-shape function $\epsilon_0(\omega)$. For a Lorentzian band Eq. (13) holds, but for an arbitrary line shape the behavior of ϵ_1 is described by $\epsilon_1=\Delta(d\epsilon_0/d\omega)$. In the neighborhood of 2.5 eV, the optical constants ϵ_0' and ϵ_0'' show a strong de-

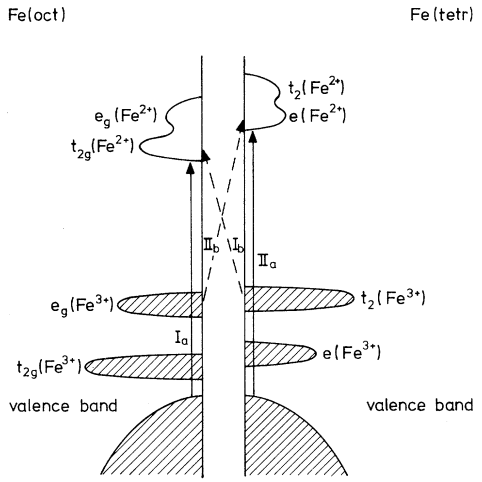

FIG. 15. Energy-level scheme for Fe(oct) and Fe(tetr) in iron garnets. Solid arrows (IA, IIa) denote the lowest oxygen-to-iron charge transfer transitions. Dashed arrows (Ib, IIb) indicate the lowest intervalence transitions within an Fe^{3+}(oct)-Fe^{3+}(tetr) pair.

pendence on frequency, making ϵ_1 larger than predicted from a symmetrical Lorentzian band. The wavelength dependences of the optical constants and Faraday rotation in this region are reminiscent of those observed for semiconductors near the band edge.

For unsubstituted YIG, ϵ_1' is positive at low photon energies. This means that the main contribution comes from a transition at higher energy with a negative peak of ϵ_1'. Considering the ϵ_1' spectrum for $x=0$ in Fig. 5, we conclude that this transition must be the peak at 4.1 eV. The contribution of this peak will, of course, be offset partially by the transitions at 4.9 and 2.8 eV of the opposite sign.

Summarizing, the following conclusion concerning the origin of the Faraday rotation in garnets can be drawn from the present ϵ_1' spectra: The major origin of the Faraday rotation shifts from a band at 4.1 eV in unsubstituted YIG to a band at 3.3 eV when bismuth is substituted. These two bands have the opposite sign for the splitting of the excited states.

D. Relation with the electronic energy-level scheme

In this section we discuss assignments of the optical absorption of bands I (2.8 eV) and II (3.3 eV).

Bands I and II have to be allowed transitions and not Fe^{3+} crystal-field transitions. This follows from the measured oscillator strength, linewidths, and the behavior of the off-diagonal tensor elements.

We will consider two types of allowed transitions[20] (see Fig. 15): (i) The transition of an electron from oxygen to iron ($Fe^{3+}+O^{2-}\rightarrow Fe^{2+}+O^{-}$). These transitions can have a band-band or an excitonic character. (ii) The transition of an electron from one iron ion to another ($2Fe^{3+}\rightarrow Fe^{2+}+Fe^{4+}$).

Until now the oxygen-to-iron charge transfers (i) have been considered by most authors[5,9] as the origin of the strong absorption bands above ~3 eV. The final state of these transitions is the iron $3d$ band, which consists of four "subbands" derived from the octahedral iron $t_{2g}(Fe^{2+})$ and $e_g(Fe^{2+})$ levels and the tetrahedral $e(Fe^{2+})$ and $t_2(Fe^{2+})$ levels. The lowest octahedral level is $t_{2g}(Fe^{2+})$ and the lowest tetrahedral level is $e(Fe^{2+})$. Consequently, the lowest band I should be interpreted as a transition to one of these two levels, which can be distinguished on the basis of their magneto-optical behavior, i.e., their ϵ_1 curves.

The excited electrons in the $t_{2g}(Fe^{2+})$ level have appreciable spin-orbit coupling which leads, in the case of ferrimagnetic ordering, to a double transition of type I (cf. Sec. V A), whereas an electron in the tetrahedral e band has, for symmetry reasons, no spin-orbit splitting and the corresponding transitions will exhibit no maximum in ϵ_1'. In unsubstituted YIG, band I has a relatively large peak in the ϵ_1' curve, corresponding to a splitting $\Delta=0.005$ eV and it should thus be assigned to the charge transfer oxygen $(2p)\rightarrow t_{2g}(Fe^{2+})$, and band II, with the negligible splitting, to the transition oxygen $2p\rightarrow e(Fe^{2+})$. In Fig. 15 a schematic energy-level diagram is given in which these possible assignments are indicated as Ia and IIa. The holes present in the oxygen $2p$ band in the final states of these transitions have spin-orbit couplings which are very small compared with those of the electrons in the $t_{2g}(Fe^{2+})$ orbitals.[18] This interpretation is supported by some results from a molecular-orbital model for the ferric oxide compounds. According to this model the lowest charge transfer of the octahedral complex is the symmetry-forbidden transition $t_{1g}(\pi)\rightarrow t_{2g}(Fe^{2+})$ whereas the lowest tetrahedral charge transfer is the allowed transition $t_1(\pi)\rightarrow e(Fe^{2+})$. $t_g(\pi)$ and $t_1(\pi)$ are energy levels derived mainly from oxygen $2p$ states near the top of the valence band. This difference in transition probability can explain the different oscillator strength of band Ia and IIa.

This assignment is also in fair agreement with the interpretations of spectra of ferric compounds given by previous authors, but two aspects are not satisfactory: The oscillator strengths are rather low for charge transfer bands and the absorption measurements of diluted Fe^{3+} compounds[19,21] such as Fe^{+} in YGaG indicate that the typical strong charge transfers occur above 4 eV, moreover, the bands such as I and II have a concentration-dependent oscillator strength. This favors assignments to transitions involving more than one Fe^{3+} ion. Therefore, we consider now transitions (ii) between

neighboring octahedral and tetrahedral Fe^{3+} ions. An attractive aspect of this interpretation is that these Fe-Fe transitions are expected at lower energies than the oxygen-iron charge transfer, since the Fe^{3+} levels are thought to be situated[10] above the oxygen valence band. A certain overlap of wave functions necessary for a transition probability is consistent with the strong magnetic interactions. Eight Fe-Fe transitions are possible. According to the usual values of 10 Dq, charge transfer energies, and known valences of iron in oxygen surroundings, the lowest valence transitions within an Fe^{3+}(oct)-Fe^{3+}(tetr) pair will be $t_2(Fe^{3+}) \rightarrow t_{2g}(Fe^{2+})$ and $e_g(Fe^{3+}) \rightarrow e(Fe^{2+})$ (see Fig. 15).

These two transitions differ again with respect to the splitting of the final state: The $e_g(Fe^{3+}) \rightarrow e(Fe^{2+})$ transition will show no splitting since the electrons or holes in orbitals with $e(e_g)$ symmetry will have no spin-orbit splitting. The transition $t_2(Fe^{3+}) \rightarrow t_{2g}(Fe^{2+})$ will show spin-orbit splitting since both the hole in the $t_2(Fe^{3+})$ orbital and the electron in the $t_{2g}(Fe^{2+})$ orbital can contribute. Therefore, in the context of this interpretation, band I will correspond to the transition $t_2(Fe^{3+}) \rightarrow t_{2g}(Fe^{2+})$ and band II to $e_g(Fe^{3+}) \rightarrow e(Fe^{2+})$. These transitions are denoted as Ib and IIb in Fig. 15. The assignment to the lowest possible intervalence bands Ib and IIb is supported by conductivity measurements[22] which show that the electrical band gap of YIG is at 2.8 eV.

In summarizing, we find that the bands below 4 eV can be explained both as oxygen-to-iron charge transfers and as iron-iron charge transfers. It is interesting that both interpretations have in common that they assign band I as a transition to the octahedral bands and band II as a transition to the tetrahedral bands; the main difference in the explanation is the initial state of the electrons in the charge transfer process. The concentration dependence of the oscillator strengths of the bands favors the interpretation as iron-iron charge transfers (Ib, IIb in Fig. 15).

The two bands at 4.1 and 4.9 eV, corresponding with the negative and positive peak of ϵ_1', respectively, are most likely due to charge transfers from oxygen to Fe(oct) and Fe(tetr), respectively.

When bismuth is substituted into the garnet lattice it is to be expected that the 6*s* and 6*p* (valence) orbitals of the rather covalent Bi ions mix with the 2*p* valence orbitals of the surrounding oxygen orbitals. A smaller mixing will also occur between the iron 3*d* orbitals and the bismuth orbitals via the intervening oxygen atoms.

This will have two effects: The oscillator strengths of the transitions in YIG (e.g., bands I and II) will increase since they can derive intensity from transitions involving the Bi ions, such as the band $^1S_0 \rightarrow {}^3P_1$ at 4.3 eV. In the second place, it is to be expected that the spin-orbit coupling of the mixed (oxygen-iron) states involved in the transitions (see Fig. 15) will increase since the bismuth 6*p* orbitals have such a high spin-orbit coupling (~ 2.1 eV).[23] This will lead to an increased splitting of the "double" transitions.

The additional spin-orbit splitting due to the bismuth ions is 0.01 eV for band I and 0.06 eV for band II. These increases, although very important for the magneto-optical rotation are still relatively small compared to the values for the bismuth 6*p* orbitals. As a consequence we do not need unrealistic high degrees of mixing of the wave functions in order to explain the magneto-optic data.

VII. CONCLUSIONS

The present work gives a quantitative analysis of the influence of bismuth upon the magneto-optic rotations of iron garnets by analyzing both the oscillator strengths and the spin-orbit coupling of two important transitions.

The results are derived from measurements on both polycrystalline materials and single-crystal films, which show a good mutual agreement.

The calculated spectra of ϵ_0 and ϵ_1 of $Y_3Fe_5O_{12}$ and $Y_{3-x}Bi_xFe_5O_{12}$ show that the optical transitions at 2.8 eV (I) and 3.3 eV (II) are mainly responsible for the remarkable increase of the Faraday rotation in the visible and near infrared on Bi substitution. The additional spin-orbit splitting for $x=1$ has been determined to be 0.01 eV for band I and 0.05 eV for band II. The bands can be assigned to electron charge transfer transitions between neighboring octahedral and tetrahedral ions. An interpretation as oxygen-iron charge transfer is also possible and a further theoretical calculation of transition probabilities of the spin- and electric-dipole-allowed transitions in concentrated iron garnets is urgently needed. In both models a relatively small admixture of bismuth 6*p* orbitals into oxygen 2*p* and iron 3*d* orbitals can account for the increased spin-orbit splitting of these transitions on bismuth substitution.

ACKNOWLEDGMENTS

It is a pleasure to thank A. W. Op den Buijs and F. R. A. van de Valk for their help with the optical measurements, M. G. J. Kamminga and M. J. G. van Hout for their assistance in preparing the samples, and C. H. M. Witmer for sputter etching some of the thin films. Stimulating discussions with R. P. van Stapele are gratefully acknowledged.

---

[1] S. Wittekoek, Th. J. A. Popma, J. M. Robertson, and P. F. Bongers, AIP Conf. Proc. 10, 1418 (1973).

[2] D. E. Lacklison, G. B. Scott, H. I. Ralph, and J. L. Page, IEEE Trans. Magn. 9, 457 (1973).

[3]H. Takeuchi, K. Shinagana, and S. Taniguchi, Jpn. J. Appl. Phys. 12, 465 (1973).
[4]W. A. Crossley, R. W. Cooper, J. L. Page, and R. P. van Stapele, Phys. Rev. 181, 896 (1969).
[5]F. J. Kahn, P. S. Pershan, and J. P. Remeika, Phys. Rev. 186, 891 (1969).
[6]P. F. Bongers and E. Zanmarchi, J. Appl. Phys. 40, 1230 (1969).
[7]S. Wittekoek and D. E. Lacklison, Phys. Rev. Lett. 28, 740 (1972).
[8]Y. R. Shen, Phys. Rev. 133, A511 (1964). Review articles concerned with the theory of magneto-optic phenomena are M. J. Freiser, IEEE Trans. Magn. 4, 152, 1968; and J. C. Suits, *ibid.* 8, 95 (1972).
[9]S. H. Wemple, S. L. Blank, J. A. Seman, and W. A. Biolsi, Phys. Rev. B 9, 2134 (1974).
[10]S. Wittekoek and T. J. A. Popma, J. Appl. Phys. 44, 5560 (1973).
[11]J. M. Robertson, S. Wittekoek, Th. J. A. Popma, and P. F. Bongers, Appl. Phys. 2, 219 (1973).
[12]S. Wittekoek, T. J. A. Popma, and J. Robertson, AIP Conf. Proc. 18, 944 (1973).
[13]S. Wittekoek and G. Rinzema, Phys. Status Solidi B 44, 849 (1971).
[14]D. M. Roessler, Br. J. Appl. Phys. 16, 119 (1965).
[15]W. Wettling, B. Andlauer, P. Koidl, J. Schneider, and W. Toksdorf, Phys. Status Solidi 59, 63 (1973).
[16]Similar formulas have been derived in Refs. 5 and 8, but we have found small errors in both.
[17]See, e.g., C. J. Ballhausen, *Introduction to Ligand Field Theory* (McGraw-Hill, New York, 1962), p. 211.
[18]A. M. Clogston, J. Appl. Phys. 31, 1989 (1960).
[19]G. B. Scott, D. E. Lacklison, and J. L. Page, Phys. Rev. B 10, 971 (1974).
[20]Recently G. B. Scott (private communication) has suggested "double-crystal-field transitions" as a third possibility for allowed transitions in this energy region.
[21]H. W. Lehmann, Z. Phys. Chem. Neue Folge 72, 279 (1970).
[22]R. Metselaar and P. K. Larsen, Solid State Commun. 15, 291 (1974); P. M. Grant and W. Ruppel, *ibid.* 5, 543 (1967); V. V. Eremenko, A. P. Kirichenko, V. N. Rubtsov, and V. S. Smirnov, Fiz. Tverd. Tela 14, 1236 (1972) [Sov. Phys.-Solid State 14, 1057 (1972)].
[23]A. B. McLay and M. F. Crawford, Phys. Rev. 44, 986 (1933).